COMPUTER METHODS IN APPLIED MECHANICS AND ENGINEERING 71 (1988) 241–258
NORTH-HOLLAND

NONLINEAR VERSIONS OF FLEXURALLY SUPERCONVERGENT ELEMENTS

Wing Kam LIU, Ted BELYTSCHKO and Jiun-Shyan CHEN
Departments of Mechanical Engineering and Civil Engineering, Northwestern University, Evanston, IL 60208, U.S.A.

Received 14 July 1986
Revised manuscript received 29 July 1988

Flexurally superconvergent four-node elements, which can achieve engineering beam accuracy with a single layer of elements through the thickness of the beam, are generalized to nonlinear problems. The Hu–Washizu variational principal in terms of the first Piola–Kirchhoff stress tensor and the deformation gradient is used in conjunction with the γ-projection to develop an efficient form of this element. Example solutions show that while there is some degradation of the accuracy in the nonlinear range, the performance of these elements still permits very coarse meshes.

1. Introduction

The four-node, incompatible-mode elements originated by Wilson, Taylor and coworkers [1, 2] can be called flexurally superconvergent in that they achieve almost perfect engineering beam accuracy with a single layer of elements. This attribute is extremely attractive in engineering practice because it permits coarse meshing in problems dominated by bending.

It has become apparent that these elements can be developed without recourse to incompatible modes [3, 4] through the use of mixed variational principles. Moreover, certain orthogonality conditions and the γ-projection [4, 5] enable these elements to be developed in a very simple and efficient manner. This makes possible a consistent and efficient development of these elements for problems with geometrical and material nonlinearities, which is the topic of this paper.

The purpose of this paper is to develop flexurally superconvergent elements for large-displacement problems. The development of such elements, as pointed out in [4], involves two requirements:

(1) the nonconstant part of the hydrostatic field must be suppressed;

(2) the nonconstant part of the shear stress field must be suppressed.

For the purpose of developing the nonlinear elements, we will use the Hu–Washizu variational principle expressed in terms of the first Piola–Kirchhoff stress tensor and the deformation gradient [6], a development of this form of the variational principle may also be found in [7]. This form has the advantage that the compatibility and equilibrium equations are linear, so that both the geometric and material nonlinearities effectively reside in the weak form, which will be called herein the constitutive law. This, in conjunction with the γ-projection, enables

the element matrices to be developed in concise forms, which, in contrast to the usual mixed or incompatible model formulations, require no matrix inversions.

The choice of these measures of stress and deformation was motivated by the fact that the problems we are interested in involve relatively small deformations but large rotations. This then entails the use of measures of stress and strain which are valid for large rotations. While the rate of deformation, or stretching, is a valid measure of strain for such problems, it is only an incremental measure, which is awkward to apply to materials with a potential, such as the Mooney–Rivlin material.

For these reasons, we have chosen a Lagrangian measure of strain, and we have selected the deformation tensor and its conjugate, the first Piola–Kirchhoff stress, because of the linearity of the equilibrium and kinematic relations.

A disadvantage of Lagrangian measures of strain is that the incompressibility relation is no longer linear; that is, incompressibility corresponds to the condition that the determinant of the tensor remain constant, whereas, in terms of the rate of deformation, incompressibility requires that the trace of the rate of deformation vanish. However, we have found that the use of deformation fields which meet the zero trace condition is sufficient to preclude locking with fully incompressible materials and full quadrature. This is illustrated by a bending problem involving a Mooney–Rivlin material.

The outline of this paper follows. In Section 2 we review the form of the Hu–Washizu principle to be used for nonlinear elasticity problems. Section 3 develops the general nonlinear finite element equations from this variational principle. In Section 4 the specific equations for the QBI element [4], an example of a flexurally superconvergent element, are given. This includes both the internal force and tangential stiffness matrices; the latter are put in the additively decomposed form of a one-point quadrature matrix and a stabilization matrix. This is followed by some example solutions in Section 5 and conclusions in Section 6.

2. Review of Hu–Washizu variational principle for nonlinear elasticity

The simplest form of the Wu–Washizu functional for nonlinear elasticity is in terms of the first Piola–Kirchhoff stress tensor and the deformation gradient. For a single element, it can be written as

$$\Pi = \int_{R_X} W(\boldsymbol{F})\, \mathrm{d}R_X - \int_{R_X} \boldsymbol{\sigma}^{\mathrm{t}}(\boldsymbol{\varepsilon} - \nabla \boldsymbol{u})\, \mathrm{d}R_X - \boldsymbol{d}^{\mathrm{t}}\boldsymbol{f}\,, \tag{2.1}$$

where $\boldsymbol{\varepsilon} = \boldsymbol{F} - \mathbf{1}$, $\boldsymbol{F}$ is the deformation gradient, $\mathbf{1}$ is the identity matrix, W is the strain energy density function, $\boldsymbol{\sigma}$ is the first Piola–Kirchhoff stress tensor (nonsymmetric), $\nabla \boldsymbol{u}$ is the displacement gradient, $\boldsymbol{d}$ is the nodal displacement matrix, $\boldsymbol{f}$ is the nodal force matrix, R_X is the initial volume, and 't' designates 'transpose'. This variational principle can be found in Washizu [6] and Nemat–Nasser [7]. For example, in a plane two-dimensional (2D) element, the column arrays of these matrices are

$$\boldsymbol{\sigma}^{\mathrm{t}} = [\sigma_{11}, \sigma_{22}, \sigma_{12}, \sigma_{21}]\,, \tag{2.2}$$

$$\boldsymbol{\varepsilon}^{\mathrm{t}} = [\varepsilon_{11}, \varepsilon_{22}, \varepsilon_{12}, \varepsilon_{21}]$$
$$\stackrel{\text{def}}{=} [F_{11} - 1, F_{22} - 1, F_{12}, F_{21}] , \tag{2.3}$$

$$\nabla \boldsymbol{u}^{\mathrm{t}} = [u_{1,1}, u_{2,2}, u_{1,2}, u_{2,1}] , \tag{2.4}$$

where a comma denotes the partial differentiation with respect to the material coordinates (X_1, X_2). The spatial coordinates (x_1, x_2) are related to the displacement by

$$\boldsymbol{x} = \boldsymbol{X} + \boldsymbol{u}(\boldsymbol{X}, t) . \tag{2.5}$$

In (2.1) $\boldsymbol{\varepsilon}$, $\boldsymbol{\sigma}$, and $\boldsymbol{u}$ are independent fields, and the variation of this Hu–Washizu functional yields

$$\delta \Pi = \int_{R_X} \delta \boldsymbol{\varepsilon}^{\mathrm{t}} \left(\frac{\partial W}{\partial \boldsymbol{F}} - \boldsymbol{\sigma} \right) \mathrm{d}\boldsymbol{R}_X - \int_{R_X} \delta \boldsymbol{\sigma}^{\mathrm{t}} (\boldsymbol{\varepsilon} - \nabla \boldsymbol{u}) \, \mathrm{d}R_X + \int_{R_X} \delta \nabla \boldsymbol{u}^{\mathrm{t}} \boldsymbol{\sigma} \, \mathrm{d}R_X - \delta \boldsymbol{d}^{\mathrm{t}} \boldsymbol{f} = 0 . \tag{2.6}$$

As a consequence of the arbitrariness of the variations $\delta\boldsymbol{\varepsilon}$, $\delta\boldsymbol{\sigma}$, and $\delta\boldsymbol{u}$, (2.6) gives the following.

Constitutive law:

$$\int_{R_X} \delta \boldsymbol{\varepsilon}^{\mathrm{t}} (\mathscr{T} - \boldsymbol{\sigma}) \, \mathrm{d}R_X = 0 , \tag{2.7}$$

where

$$\mathscr{T}^{\mathrm{t}} = [\mathscr{T}_{11}, \mathscr{T}_{22}, \mathscr{T}_{12}, \mathscr{T}_{21}] , \tag{2.8}$$

$$\left(\frac{\partial W}{\partial \boldsymbol{F}} \right)^{\mathrm{t}} = \left[\frac{\partial W}{\partial F_{11}}, \frac{\partial W}{\partial F_{22}}, \frac{\partial W}{\partial F_{12}}, \frac{\partial W}{\partial F_{21}} \right] , \tag{2.9}$$

and

$$\mathscr{T} \stackrel{\text{def}}{=} \frac{\partial W}{\partial \boldsymbol{F}} = \text{a given function of } \boldsymbol{F} . \tag{2.10}$$

Compatibility equation:

$$\int_{R_X} \delta \boldsymbol{\sigma}^{\mathrm{t}} (\boldsymbol{\varepsilon} - \nabla \boldsymbol{u}) \, \mathrm{d}R_X = 0 . \tag{2.11}$$

Equilibrium:

$$\int_{R_X} \delta \nabla \boldsymbol{u}^{\mathrm{t}} \boldsymbol{\sigma} \, \mathrm{d}R_X - \delta \boldsymbol{d}^{\mathrm{t}} \boldsymbol{f} = 0 . \tag{2.12}$$

As can be seen from (2.7)–(2.12), the Euler–Lagrange equations are very similar to those of linear elasticity, and in particular, the compatibility and equilibrium equations are both linear; the nonlinearity resides entirely in (2.7). The two major differences are that a nonlinear function and both the symmetric and skew-symmetric parts of the displacement

gradients have to be used (i.e. four strain and stress components instead of three strain and stress components). Only (2.7) is a nonlinear equation which arises from a nonlinear constitutive relation. For purposes of developing the tangential stiffness matrices, we consider a linearization of (2.6).

The linearized Hu–Washizu variational equation (2.6) is

$$\int_{R_X} \delta\boldsymbol{\varepsilon}^{\mathrm{t}}(\boldsymbol{C}^1\,\Delta\boldsymbol{\varepsilon} - \Delta\boldsymbol{\sigma})\,\mathrm{d}R_X - \int_{R_X} \delta\boldsymbol{\sigma}^{\mathrm{t}}(\Delta\boldsymbol{\varepsilon} - \nabla\,\Delta\boldsymbol{u})\,\mathrm{d}R_X + \int_{R_X} \delta\nabla\boldsymbol{u}^{\mathrm{t}}\,\Delta\boldsymbol{\sigma}\,\mathrm{d}R_X - \delta\boldsymbol{d}^{\mathrm{t}}\,\Delta\boldsymbol{f} = 0\,, \tag{2.13}$$

where Δ denotes the increment and $\boldsymbol{C}^1$ is the first elasticity tensor. It is defined as

$$\boldsymbol{C}^1 = \frac{\partial^2 W}{\partial \boldsymbol{F}\,\partial \boldsymbol{F}}\,, \tag{2.14}$$

and it is related to the second elasticity tensor $\boldsymbol{C}^2$ and the second Piola–Kirchhoff stress tensor (symmetric) $\boldsymbol{S}$ by

$$C^1_{ijkl} = \delta_{ik}S_{jl} + 2F_{ip}F_{kq}C^2_{pjql} \overset{\text{def}}{=} T_{ijkl} + D_{ijkl}\,, \tag{2.15}$$

where δ_{ik} are the components of the Kronecker delta and the components of the second elasticity tensor are

$$2C^2_{pqrs} = \frac{\partial^2 W}{\partial E_{pq}\,\partial E_{rs}}\,, \tag{2.16}$$

where E_{pq} are the components of the Lagrangian strain tensor. The stationary conditions in (2.13) yield the following.

Linearized constitutive law:

$$\int_{R_X} \delta\boldsymbol{\varepsilon}^{\mathrm{t}}(\boldsymbol{C}^1\,\Delta\boldsymbol{\varepsilon} - \Delta\boldsymbol{\sigma})\,\mathrm{d}R_X = 0\,. \tag{2.17}$$

Linearized compatibility equation:

$$\int_{R_X} \delta\boldsymbol{\sigma}^{\mathrm{t}}(\Delta\boldsymbol{\varepsilon} - \nabla\,\Delta\boldsymbol{u})\,\mathrm{d}R_X = 0\,. \tag{2.18}$$

Linearized equilibrium:

$$\int_{R_X} \delta\nabla\boldsymbol{u}^{\mathrm{t}}\,\Delta\boldsymbol{\sigma}\,\mathrm{d}R_X - \delta\boldsymbol{d}^{\mathrm{t}}\,\Delta\boldsymbol{f} = 0\,. \tag{2.19}$$

3. Mixed finite element formulation

In the mixed finite element formulation, $\boldsymbol{u}$ is approximated by C^0 functions, and $\boldsymbol{\varepsilon}$ and $\boldsymbol{\sigma}$ are approximated by C^{-1} functions in the form

$$\boldsymbol{u} = \boldsymbol{N}(\boldsymbol{X})\boldsymbol{d}\,, \qquad \Delta\boldsymbol{u} = \boldsymbol{N}(\boldsymbol{X})\,\Delta\boldsymbol{d}\,, \tag{3.1}$$

$$\boldsymbol{\varepsilon} = \boldsymbol{E}(\boldsymbol{X})\boldsymbol{e}\,, \qquad \Delta\boldsymbol{\varepsilon} = \boldsymbol{E}(\boldsymbol{X})\,\Delta\boldsymbol{e}\,, \tag{3.2}$$

$$\boldsymbol{\sigma} = \boldsymbol{S}(\boldsymbol{X})\boldsymbol{s}\,, \qquad \Delta\boldsymbol{\sigma} = \boldsymbol{S}(\boldsymbol{X})\,\Delta\boldsymbol{s}\,, \tag{3.3}$$

where $\boldsymbol{N}$, $\boldsymbol{E}$, and $\boldsymbol{S}$ are the displacement, strain, and stress interpolation functions, respectively. They are functions of the material coordinates $(\boldsymbol{X})$; $\boldsymbol{d}$, $\boldsymbol{e}$, and $\boldsymbol{s}$ are the corresponding interpolant vectors. The discrete gradient operator (with respect to $\boldsymbol{X}$) is denoted by $\boldsymbol{B}$ so that

$$\nabla\boldsymbol{u} = \boldsymbol{B}(\boldsymbol{X})\boldsymbol{d}\,, \qquad \nabla\,\Delta\boldsymbol{u} = \boldsymbol{B}(\boldsymbol{X})\,\Delta\boldsymbol{d}\,. \tag{3.4}$$

It is noted that even though (3.1)–(3.4) resemble those of the linear elasticity formulation (see, for example, [4]), these element strain, stress, and gradient vectors have more components. For example, the element strain and stress vectors have four and nine components (instead of three and six components) for plane two-dimensional (2D) and three-dimensional (3D) elements, respectively.

Substituting the above approximations into (2.6) and (2.13), the two sets of stationary conditions are obtained using the arbitrariness of $\delta\boldsymbol{e}$, $\delta\boldsymbol{s}$, and $\delta\boldsymbol{d}$.

Constitutive law:

$$\boldsymbol{q} - \bar{\boldsymbol{E}}^{\mathrm{t}}\boldsymbol{s} = \boldsymbol{0}\,, \qquad \bar{\boldsymbol{C}}^{1}\,\Delta\boldsymbol{e} - \bar{\boldsymbol{E}}^{\mathrm{t}}\,\Delta\boldsymbol{s} = \boldsymbol{0}\,. \tag{3.5}$$

Compatibility equation:

$$\bar{\boldsymbol{E}}\boldsymbol{e} - \bar{\boldsymbol{B}}\boldsymbol{d} = \boldsymbol{0}\,, \qquad \bar{\boldsymbol{E}}\,\Delta\boldsymbol{e} - \bar{\boldsymbol{B}}\,\Delta\boldsymbol{d} = \boldsymbol{0}\,. \tag{3.6}$$

Equilibrium:

$$\bar{\boldsymbol{B}}^{\mathrm{t}}\boldsymbol{s} - \boldsymbol{f} = \boldsymbol{0}\,, \qquad \bar{\boldsymbol{B}}^{\mathrm{t}}\,\Delta\boldsymbol{s} - \Delta\boldsymbol{f} = \boldsymbol{0}\,, \tag{3.7}$$

where

$$\boldsymbol{q} = \int_{R_X} \boldsymbol{E}^{\mathrm{t}}\boldsymbol{\mathcal{T}}\,\mathrm{d}\boldsymbol{R}_X\,, \qquad \bar{\boldsymbol{C}}^{1} = \int_{R_X} \boldsymbol{E}^{\mathrm{t}}\boldsymbol{C}^{1}\boldsymbol{E}\,\mathrm{d}R_X\,, \tag{3.8}$$

and

$$\bar{\boldsymbol{E}} = \int_{R_X} \boldsymbol{S}^{\mathrm{t}}\boldsymbol{E}\,\mathrm{d}R_X\,, \qquad \bar{\boldsymbol{B}} = \int_{R_X} \boldsymbol{S}^{\mathrm{t}}\boldsymbol{B}\,\mathrm{d}R_X\,. \tag{3.9}$$

The parameters $\Delta\boldsymbol{e}$ and $\Delta\boldsymbol{s}$ and the element *tangent* stiffness matrix $\boldsymbol{K}$ are now obtained from (3.5)–(3.7):

$$\Delta\boldsymbol{e} = \bar{\boldsymbol{E}}^{-1}\bar{\boldsymbol{B}}\,\Delta\boldsymbol{d}\,, \qquad \Delta\boldsymbol{s} = \bar{\boldsymbol{E}}^{-\mathrm{t}}\bar{\boldsymbol{C}}^{1}\bar{\boldsymbol{E}}^{-1}\bar{\boldsymbol{B}}\,\Delta\boldsymbol{d}\,, \tag{3.10}$$

$$\boldsymbol{K} = \boldsymbol{K}^D + \boldsymbol{K}^G , \tag{3.11}$$

where the stiffness is separated into two parts: $\boldsymbol{K}^D$ which is due to the material modulus matrix,

$$\boldsymbol{K}^D = \bar{\boldsymbol{B}}^{\mathrm{t}} \bar{\boldsymbol{E}}^{-\mathrm{t}} \bar{\boldsymbol{D}} \bar{\boldsymbol{E}}^{-1} \bar{\boldsymbol{B}} , \tag{3.12}$$

and $\boldsymbol{K}^G$ which is due to the initial stress matrix,

$$\boldsymbol{K}^G = \bar{\boldsymbol{B}}^{\mathrm{t}} \bar{\boldsymbol{E}}^{-\mathrm{t}} \bar{\boldsymbol{T}} \bar{\boldsymbol{E}}^{-1} \bar{\boldsymbol{B}} . \tag{3.13}$$

$\bar{\boldsymbol{D}}$ and $\bar{\boldsymbol{T}}$ are obtained from substituting (2.15) into (3.8),

$$\bar{\boldsymbol{D}} = \int_{R_X} \boldsymbol{E}^{\mathrm{t}} \boldsymbol{D} \boldsymbol{E} \, \mathrm{d}R_X , \qquad \bar{\boldsymbol{T}} = \int_{R_X} \boldsymbol{E}^{\mathrm{t}} \boldsymbol{T} \boldsymbol{E} \, \mathrm{d}R_X . \tag{3.14}$$

Finally, $\boldsymbol{f}^{\mathrm{int}}$ is given by

$$\boldsymbol{f}^{\mathrm{int}} = \bar{\boldsymbol{B}}^{\mathrm{t}} \bar{\boldsymbol{E}}^{-\mathrm{t}} \boldsymbol{q} . \tag{3.15}$$

It can be shown that the assembled linearized equilibrium equation is

$$(\boldsymbol{K}^D + \boldsymbol{K}^G) \, \Delta \boldsymbol{d} = \Delta \boldsymbol{f}^{\mathrm{ext}} , \tag{3.16}$$

where $\boldsymbol{f}^{\mathrm{int}}$ is assembled from the element nodal force matrices, and $\boldsymbol{f}^{\mathrm{ext}}$ is the assembled external nodal force vector. In summary, the solution procedure is as follows.

Step a. Initialization.
Step b. Compute $\boldsymbol{e} = \bar{\boldsymbol{E}}^{-1} \bar{\boldsymbol{B}} \boldsymbol{d}$ (a linear relation).
Step c. Define $\boldsymbol{q} = \int_{R_X} \boldsymbol{E}^{\mathrm{t}} \mathcal{T}(\boldsymbol{e}) \, \mathrm{d}R_X$ (a nonlinear relation).
Step d. Compute $\boldsymbol{s} = \bar{\boldsymbol{E}}^{-\mathrm{t}} \boldsymbol{q}$ (a linear relation).
Step e. Compute $\boldsymbol{K}^D$, $\boldsymbol{K}^G$, $\boldsymbol{f}^{\mathrm{ext}}$, and $\boldsymbol{f}^{\mathrm{int}}$.
Step f. Solve for $\Delta \boldsymbol{d}$ (equations (3.15) and (3.16), respectively).
Step g. Convergence check: is $\boldsymbol{f}^{\mathrm{ext}} = \boldsymbol{f}^{\mathrm{int}}$?
Step h. $\boldsymbol{d}$ is replaced by $\boldsymbol{d} + \Delta \boldsymbol{d}$, and go to Step b.

4. Explicit expressions for $\boldsymbol{K}^D$, $\boldsymbol{K}^G$, and $\boldsymbol{f}^{\mathrm{int}}$

A family of linear γ-elements, which consists essentially of uniformly reduced integration elements with a consistent stabilization to avoid spurious singular modes, has been reported in [4, 8, 9]. In this section, the construction of stabilization matrices for $\boldsymbol{K}^D$, $\boldsymbol{K}^G$, and $\boldsymbol{f}^{\mathrm{int}}$ for the QBI element [4] is described. These matrices are decomposed in the form

$$\boldsymbol{K}^D = \boldsymbol{K}^D_0 + \boldsymbol{K}^D_{\mathrm{stab}} , \tag{4.1}$$

$$\boldsymbol{K}^G = \boldsymbol{K}_0^G + \boldsymbol{K}_{\text{stab}}^G , \tag{4.2}$$

and

$$\boldsymbol{f}^{\text{int}} = \boldsymbol{f}_0 + \boldsymbol{f}_{\text{stab}} . \tag{4.3}$$

Since the development of these stabilization matrices is similar to that of the linear theory, the tangent matrices and the $\boldsymbol{f}^{int}$ vector are given by (for simplicity, only the 2D plane elements are described)

$$\boldsymbol{K}_{\text{stab}} = \begin{bmatrix} c_1 \boldsymbol{\gamma}\boldsymbol{\gamma}^{\text{t}} & c_2 \boldsymbol{\gamma}\boldsymbol{\gamma}^{\text{t}} \\ c_2 \boldsymbol{\gamma}\boldsymbol{\gamma}^{\text{t}} & c_3 \boldsymbol{\gamma}\boldsymbol{\gamma}^{\text{t}} \end{bmatrix} \tag{4.4}$$

and

$$\boldsymbol{f}_{\text{stab}} = \begin{Bmatrix} c_4 \boldsymbol{\gamma} \\ c_5 \boldsymbol{\gamma} \end{Bmatrix} . \tag{4.5}$$

The choice of the coefficients c_i depends on the interpolant functions ($\boldsymbol{N}$, $\boldsymbol{E}$, and $\boldsymbol{S}$). The *nonlinear* version of the quintessential bending incompressible (QBI) element described in [4] is constructed as follows.

4.1. Displacements

The displacement field is given in terms of the γ-operator for hourglass control [4, 5],

$$u_i = [\boldsymbol{\Delta}^{\text{t}} + X_j \boldsymbol{b}_j^{\text{t}} + \hbar \boldsymbol{\gamma}^{\text{t}}] \boldsymbol{d}_i , \quad i, j = 1, 2 , \tag{4.6a}$$

where $\hbar = \xi\eta$; repeated subscripts signify sums and

$$\boldsymbol{\gamma}^{\text{t}} = \tfrac{1}{4}[\boldsymbol{h} - (\boldsymbol{h}\boldsymbol{X}_i)\boldsymbol{b}_i] . \tag{4.6b}$$

The original area of the quadrilateral element is

$$A = \tfrac{1}{4}[(\boldsymbol{\xi}^{\text{t}}\boldsymbol{X})(\boldsymbol{\eta}^{\text{t}}\boldsymbol{Y}) - (\boldsymbol{\xi}^{\text{t}}\boldsymbol{Y})(\boldsymbol{\eta}^{\text{t}}\boldsymbol{X})] , \tag{4.7}$$

$$\boldsymbol{X}_1^{\text{t}} = \boldsymbol{X}^{\text{t}} = [X_1, X_2, X_3, X_4] , \tag{4.8}$$

$$\boldsymbol{X}_2^{\text{t}} = \boldsymbol{Y}^{\text{t}} = [Y_1, Y_2, Y_3, Y_4] , \tag{4.9}$$

$$\boldsymbol{\xi}^{\text{t}} = [-1, 1, 1, -1] , \tag{4.10}$$

$$\boldsymbol{\eta}^{\text{t}} = [-1, -1, 1, 1] . \tag{4.11}$$

The vectors $\boldsymbol{b}_i$ are the derivatives of the shape functions evaluated at $\xi = \eta = 0$:

$$\boldsymbol{b}_1^{\text{t}} = \frac{\partial \boldsymbol{N}(\boldsymbol{0})}{\partial X} = \frac{1}{2A} [Y_{24}, Y_{31}, Y_{42}, Y_{13}] , \tag{4.12}$$

$$\boldsymbol{b}_2^{\text{t}} = \frac{\partial \boldsymbol{N}(\boldsymbol{0})}{\partial Y} = \frac{1}{2A} [X_{42}, X_{13}, X_{24}, X_{31}] , \tag{4.13}$$

where

$$X_{IJ} = X_I - X_J\,, \tag{4.14}$$

$$Y_{IJ} = Y_I - Y_J\,, \tag{4.15}$$

$$\boldsymbol{\Delta}^{\mathrm{t}} = \tfrac{1}{4}[\boldsymbol{s} - (\boldsymbol{s}\boldsymbol{X}_j)\boldsymbol{b}_j]\,, \qquad \boldsymbol{s}^{\mathrm{t}} = [1, 1, 1, 1]\,, \tag{4.16}$$

$$\boldsymbol{h}^{\mathrm{t}} = [1, -1, 1, -1]\,. \tag{4.17}$$

The displacement gradient field is

$$\nabla \boldsymbol{u} = \begin{Bmatrix} u_{1,1} \\ u_{2,2} \\ u_{1,2} \\ u_{2,1} \end{Bmatrix} = \begin{bmatrix} \boldsymbol{b}_1^{\mathrm{t}} + \boldsymbol{h}_{,X}\boldsymbol{\gamma}^{\mathrm{t}} & \boldsymbol{0} \\ \boldsymbol{0} & \boldsymbol{b}_2^{\mathrm{t}} + \boldsymbol{h}_{,Y}\boldsymbol{\gamma}^{\mathrm{t}} \\ \boldsymbol{b}_2^{\mathrm{t}} + \boldsymbol{h}_{,Y}\boldsymbol{\gamma}^{\mathrm{t}} & \boldsymbol{0} \\ \boldsymbol{0} & \boldsymbol{b}_1^{\mathrm{t}} + \boldsymbol{h}_{,X}\boldsymbol{\gamma}^{\mathrm{t}} \end{bmatrix} \begin{Bmatrix} \boldsymbol{d}_1 \\ \boldsymbol{d}_2 \end{Bmatrix} = \boldsymbol{B}\boldsymbol{d}\,. \tag{4.18}$$

4.2. Strains

The strain interpolation is given by

$$\boldsymbol{\varepsilon} = \boldsymbol{E}\boldsymbol{e}\,, \qquad \boldsymbol{\varepsilon} = [\varepsilon_{11}, \varepsilon_{22}, \varepsilon_{12}, \varepsilon_{21}]^{\mathrm{t}}\,. \tag{4.19}$$

The nonlinear QBI strain interpolant matrix is

$$\boldsymbol{E} = \begin{bmatrix} 1 & 0 & 0 & 0 & \boldsymbol{h}_{,X} & -\bar{\nu}\boldsymbol{h}_{,Y} \\ 0 & 1 & 0 & 0 & -\bar{\nu}\boldsymbol{h}_{,X} & \boldsymbol{h}_{,Y} \\ 0 & 0 & 1 & 0 & 0 & 0 \\ 0 & 0 & 0 & 1 & 0 & 0 \end{bmatrix}, \tag{4.20}$$

where $\bar{\nu} = \nu$ for plane stress, $\bar{\nu} = \nu/(1-\nu)$ for plane strain, and ν is Poisson's ratio.

4.3. Stresses

The stress interpolation is given by

$$\boldsymbol{\sigma} = \boldsymbol{S}\boldsymbol{s}\,, \qquad \boldsymbol{\sigma} = [\sigma_{11}, \sigma_{22}, \sigma_{12}, \sigma_{21}]^{\mathrm{t}}\,, \tag{4.21}$$

where

$$\boldsymbol{S} = \begin{bmatrix} 1 & 0 & 0 & 0 & \boldsymbol{h}_{,X} & 0 \\ 0 & 1 & 0 & 0 & 0 & \boldsymbol{h}_{,Y} \\ 0 & 0 & 1 & 0 & 0 & 0 \\ 0 & 0 & 0 & 1 & 0 & 0 \end{bmatrix}. \tag{4.22}$$

4.4. Constitutive law

Because $\mathcal{T} = \partial W/\partial \boldsymbol{F}$ is in general a nonlinear function, numerical integration has to be used, however, to evaluate the *vector* $\boldsymbol{q}$ with two or more quadrature points; that is

$$\boldsymbol{q} = \sum_{I=1}^{\mathrm{NINT}} \boldsymbol{E}^{\mathrm{t}}(\boldsymbol{\xi}_I)\mathcal{T}(\boldsymbol{\xi}_I)J(\boldsymbol{\xi}_I)W_I\,. \tag{4.23}$$

ξ_l and W_l are the integration points and weights, respectively; J is the Jacobian, and NINT ≥ 2.

Since $\boldsymbol{D}$ and $\boldsymbol{T}$ (see (2.15)) are used to obtain the tangent matrices, it suffices to use the weighted average $\boldsymbol{D}$ and $\boldsymbol{T}$,

$$\tilde{\boldsymbol{D}} = \sum_{l=1}^{\text{NINT}} w_l \boldsymbol{D}(\xi_l), \qquad \tilde{\boldsymbol{T}} = \sum_{l=1}^{\text{NINT}} w_l \boldsymbol{T}(\xi_l), \tag{4.24}$$

where w_l are weighting factors. With this approximation, $\boldsymbol{K}^D$ and $\boldsymbol{K}^G$ can be put into the forms given by (4.1) and (4.2), respectively.

The explicit expressions for $\bar{\boldsymbol{E}}$ and $\bar{\boldsymbol{B}}$ are

$$\bar{\boldsymbol{E}} = \left[\begin{array}{c|cc} A\mathbf{1}_{4\times 4} & \mathbf{0}_{4\times 2} & \\ \hline \mathbf{0}_{2\times 4} & H_{XX} & -\bar{\nu}H_{XY} \\ & -\bar{\nu}H_{XY} & H_{YY} \end{array}\right], \tag{4.25}$$

where the numerical subscripts denote the orders of the submatrices;

$$\bar{\boldsymbol{B}} = \left[\begin{array}{cc} A\boldsymbol{b}_1^{\mathrm{t}} & \mathbf{0} \\ \mathbf{0} & A\boldsymbol{b}_2^{\mathrm{t}} \\ A\boldsymbol{b}_2^{\mathrm{t}} & \mathbf{0} \\ \mathbf{0} & A\boldsymbol{b}_1^{\mathrm{t}} \\ \hline H_{XX}\boldsymbol{\gamma}^{\mathrm{t}} & \mathbf{0} \\ \mathbf{0} & H_{YY}\boldsymbol{\gamma}^{\mathrm{t}} \end{array}\right], \tag{4.26}$$

where H_{XX}, H_{XY}, and H_{YY} are given by

$$H_{ij} = \int_{R_X} \hbar_{,i}\hbar_{,j}\,\mathrm{d}R_X . \tag{4.27}$$

The $\bar{\boldsymbol{D}}$ and $\bar{\boldsymbol{T}}$ matrices are

$$\bar{\boldsymbol{D}} = \left[\begin{array}{c|cc} A\tilde{\boldsymbol{D}}_{4\times 4} & \mathbf{0}_{4\times 2} & \\ \hline \mathbf{0}_{2\times 4} & \tilde{\alpha}^D_{XX}H_{XX} & \tilde{\alpha}^D_{XY}H_{XY} \\ & \tilde{\alpha}^D_{YX}H_{XY} & \tilde{\alpha}^D_{YY}H_{YY} \end{array}\right], \tag{4.28}$$

$$\bar{\boldsymbol{T}} = \left[\begin{array}{c|cc} A\tilde{\boldsymbol{T}}_{4\times 4} & \mathbf{0}_{4\times 2} & \\ \hline \mathbf{0}_{2\times 4} & \tilde{\alpha}^G_{XX}H_{XX} & \tilde{\alpha}^G_{XY}H_{XY} \\ & \tilde{\alpha}^G_{YX}H_{XY} & \tilde{\alpha}^G_{YY}H_{YY} \end{array}\right]. \tag{4.29}$$

With these preliminaries, the explicit expressions for the one-point $\boldsymbol{K}^D_0$, $\boldsymbol{K}^G_0$, and $\boldsymbol{f}_0$ are as

follows (in terms of $\boldsymbol{b}_1$ and $\boldsymbol{b}_2$):

$$\boldsymbol{K}_0^D = A\left[\begin{array}{c|c} \tilde{D}_{11}\boldsymbol{b}_1\boldsymbol{b}_1^t + \tilde{D}_{13}\boldsymbol{b}_1\boldsymbol{b}_2^t + \tilde{D}_{31}\boldsymbol{b}_2\boldsymbol{b}_1^t + \tilde{D}_{33}\boldsymbol{b}_2\boldsymbol{b}_2^t & \tilde{D}_{12}\boldsymbol{b}_1\boldsymbol{b}_2^t + \tilde{D}_{14}\boldsymbol{b}_1\boldsymbol{b}_1^t + \tilde{D}_{32}\boldsymbol{b}_2\boldsymbol{b}_2^t + \tilde{D}_{34}\boldsymbol{b}_2\boldsymbol{b}_1^t \\ \hline \tilde{D}_{21}\boldsymbol{b}_2\boldsymbol{b}_1^t + \tilde{D}_{23}\boldsymbol{b}_2\boldsymbol{b}_2^t + \tilde{D}_{41}\boldsymbol{b}_1\boldsymbol{b}_1^t + \tilde{D}_{43}\boldsymbol{b}_1\boldsymbol{b}_2^t & \tilde{D}_{22}\boldsymbol{b}_2\boldsymbol{b}_2^t + \tilde{D}_{24}\boldsymbol{b}_2\boldsymbol{b}_1^t + \tilde{D}_{42}\boldsymbol{b}_1\boldsymbol{b}_2^t + \tilde{D}_{44}\boldsymbol{b}_1\boldsymbol{b}_1^t \end{array}\right]. \tag{4.30}$$

The $\boldsymbol{K}_0^G$ matrix is similarly defined with $\tilde{\boldsymbol{D}}$ replaced by $\tilde{\boldsymbol{T}}$.

Similarly, f_0 can be shown to be

$$f_0 = \begin{Bmatrix} q_1\boldsymbol{b}_1 + q_3\boldsymbol{b}_2 \\ q_2\boldsymbol{b}_2 + q_4\boldsymbol{b}_1 \end{Bmatrix}, \tag{4.31}$$

where q_i is the ith component of array $\boldsymbol{q}$.

The explicit expression for the stabilization matrices $\boldsymbol{K}_{\text{stab}}^D$, $\boldsymbol{K}_{\text{stab}}^G$, and f_{stab} are

$$\boldsymbol{K}_{\text{stab}}^D = \begin{bmatrix} c_1^D\boldsymbol{\gamma}\boldsymbol{\gamma}^t & c_2^D\boldsymbol{\gamma}\boldsymbol{\gamma}^t \\ c_2^D\boldsymbol{\gamma}\boldsymbol{\gamma}^t & c_3^D\boldsymbol{\gamma}\boldsymbol{\gamma}^t \end{bmatrix}, \tag{4.32}$$

$$\boldsymbol{K}_{\text{stab}}^G = \begin{bmatrix} c_1^G\boldsymbol{\gamma}\boldsymbol{\gamma}^t & c_2^G\boldsymbol{\gamma}\boldsymbol{\gamma}^t \\ c_2^G\boldsymbol{\gamma}\boldsymbol{\gamma}^t & c_3^G\boldsymbol{\gamma}\boldsymbol{\gamma}^t \end{bmatrix}, \tag{4.33}$$

$$f_{\text{stab}} = \begin{Bmatrix} c_5\boldsymbol{\gamma} \\ c_6\boldsymbol{\gamma} \end{Bmatrix}. \tag{4.34}$$

The coefficients are given in Appendix A. Note that the geometric stabilization matrix has the same form as the linearized stabilization matrix $\boldsymbol{K}^D$.

5. Numerical examples

Two material laws have been used in these examples:

(1) a Mooney–Rivlin material for isotropic, incompressible rubber;

(2) a Saint Venant–Kirchhoff elastic model.

For the Mooney–Rivlin material, the strain energy is given by

$$W = c_1(I_1 - 3) + c_2(I_2 - 3), \tag{5.1}$$

and in addition, we have the incompressibility constraint

$$I_3 = 1, \tag{5.2}$$

where

$$I_3 = \det(\boldsymbol{C}), \tag{5.3}$$

and I_1 and I_2 are invariants of the Green deformation tensor, which are given by

$$I_1 = \text{trace}(C_{ij}) = C_{ii} , \tag{5.4}$$

$$I_2 = \tfrac{1}{2}(C_{ij}C_{ij} - I_1^2) . \tag{5.5}$$

The incompressibility constraint (5.2) is applied by a penalty method; to implement the penalty, it is appended to the strain energy (5.1), yielding

$$W = c_1(I_1 - 3) + c_2(I_2 - 3) + \tfrac{1}{2}\lambda^*(\ln I_3)^2 . \tag{5.6}$$

The second Piola–Kirchhoff stress is then given by

$$S_{ij} = \frac{\partial W}{\partial E_{ij}} = 2[c_1\delta_{ij} + c_2(C_{kk}\delta_{ij} - C_{ij})] - 2(p_0 - \lambda^* \ln I_3)C_{ij}^{-1} , \tag{5.7a}$$

where

$$p_0 = c_1 + 2c_2 . \tag{5.7b}$$

The second elasticity tensor $\boldsymbol{C}^2$ is then obtained using (2.16), which gives

$$C^2_{ijkl} = 2c_2\delta_{ij}\delta_{kl} - c_2(\delta_{ik}\delta_{jl} + \delta_{il}\delta_{jk}) + p(C^{-1}_{ik}C^{-1}_{jl} + C^{-1}_{il}C^{-1}_{jk}) + 2\lambda^* C^{-1}_{ij}C^{-1}_{kl} , \tag{5.8a}$$

where

$$p = p_0 - \lambda^* \ln I_3 . \tag{5.8b}$$

The remaining constitutive tensors can be found from (2.15).

For the Saint Venant–Kirchhoff nonlinear model, the strain energy function W is given in terms of a matrix $\boldsymbol{C}^2$ by

$$W = C^2_{pqrs}E_{pq}E_{rs} , \tag{5.9}$$

where

$$2C^2_{pqrs} = \lambda\delta_{pq}\delta_{rs} + \mu(\delta_{pr}\delta_{qs} + \delta_{ps}\delta_{qr}) , \tag{5.10}$$

where λ and μ are the Lamé constants.

The $\tilde{\boldsymbol{D}}$ and $\tilde{\boldsymbol{T}}$ matrices are evaluated at the two integration points, $(\xi, \eta) = (1/\sqrt{3}, 1/\sqrt{3})$ and $(-1/\sqrt{3}, -1/\sqrt{3})$, and the weight factors w_1 and w_2 are set to 2. All beams are of unit width.

EXAMPLE 5.1. Linearized buckling analysis of a cantilever beam. The problem statement of the linearized buckling of a cantilever beam is depicted in Fig. 1. The eigenvalue problem solved is

$$\boldsymbol{K}^D\boldsymbol{d} = \lambda\boldsymbol{K}^G\boldsymbol{d}, \tag{5.11}$$

where $\boldsymbol{K}^G$ is constructed using the stress arising from a linear solution. The first bifurcation load as well as the analytic (engineering beam) solution for various finite element meshes are

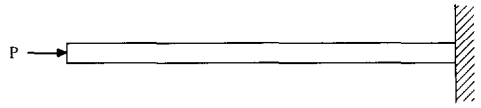

LENGTH: L=20

MOMENT OF INERTIA: $I=1\times1^3/12$

YOUNG'S MODULUS: $E=1.0\times10^6$

POISSON'S RATIO: $\nu=0.0$

Fig. 1. Problem description for Example 5.1: Linearized buckling analysis of a cantilever beam.

tabulated in Table 1. It can be seen that the QBI converges very quickly. By comparison, the selective-reduced integration (SRI) element (reduced volumetric, full deviatoric) and the full integration (FI) element are not even close to the engineering beam solution.

EXAMPLE 5.2. Large deflection of a cantilever beam subjected to a tip shear load. A cantilever beam subjected to a transverse load P was analyzed using 10×1, 20×2, and 40×4 element meshes for both the QBI and SRI elements. The problem statement as well as the results are given in Fig. 2. The finite element solutions are compared to the analytic solution [10], in which the shear deformation is neglected. While the accuracy of a coarse mesh is almost perfect in the linear range, the coarse meshes deviate somewhat in the nonlinear range. The QBI element is far superior to the SRI element for each of the meshes.

EXAMPLE 5.3. Shallow arch under a concentrated load. This problem is taken from [11]; the geometry is defined by the radius R and the subtended angle φ. The problem statement is depicted in Fig. 3. Symmetric 5×1 and 10×2 element meshes are used for half of the beam (symmetry is used), and the finite element solutions are compared with the analytic solution [12]. In this problem, excellent accuracy is achieved by the QBI element, even with a very coarse mesh.

Table 1
Buckling load of a cantilever beam

	Buckling load		
Number of elements	QBI	SRI	FI
2×1	570.9	27326.0	27546.0
5×1	521.7	4430.6	4657.4
10×1	515.3	1315.3	1542.9
10×2	515.3	1485.9	1542.8
20×1	513.7	542.4	770.2
20×4	513.8	754.9	769.5
30×1	513.9	399.5	627.4
40×1	513.9	349.5	577.4
Analytic	514.0		

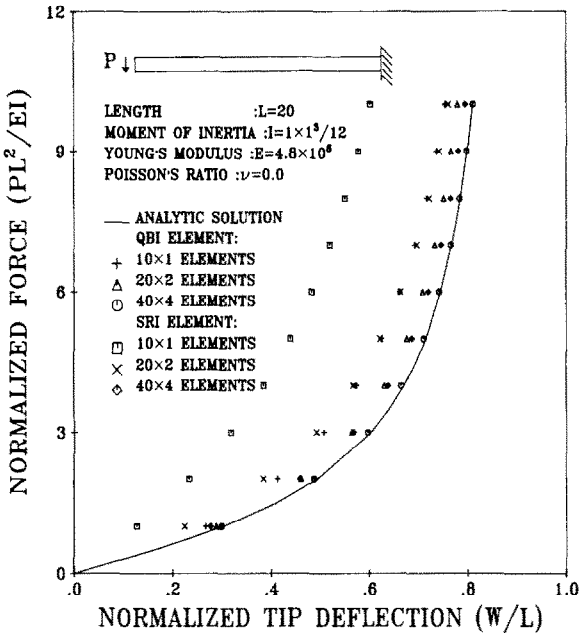

Fig. 2. Problem description and solutions for QBI and SRI elements for Example 5.2: Large deflection of beam.

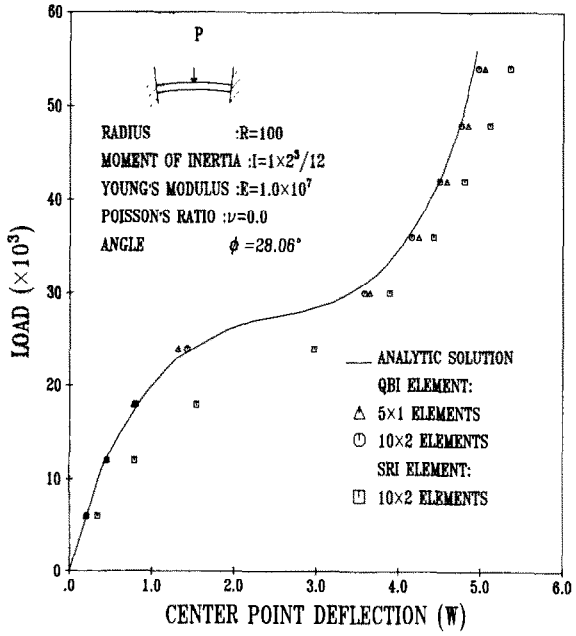

Fig. 3. Problem description and solutions for QBI and SRI elements for Example 5.3: Shallow arch under a point load.

EXAMPLE 5.4. Post-buckling analysis of an imperfect column. An initially tilted column is subjected to an axial force P. The problem definition and the finite element results as well as the analytic solution [13] are given in Fig. 4. This problem again requires a relatively fine mesh for accuracy in the nonlinear range.

EXAMPLE 5.5. Mooney–Rivlin beam. A cantilever beam as shown in Fig. 5 was subjected to an end moment by applying nodal forces equivalent to a linearly varying normal traction with zero net resultant. Note that the forces move with the beam so that they are always tangent to the top and bottom. The problem was analyzed using meshes of 10×1, 20×1, and 40×2 QBI elements.

An exact solution has been given by Rivlin [14]. The tip moment M is given by

$$M = (c_1 + c_2)\left[2a\kappa - \tfrac{1}{2}r_0^2 \ln \frac{\kappa + 2a}{\kappa - 2a}\right], \tag{5.12}$$

$$\kappa = \sqrt{4a^2 + r_0^2}, \tag{5.13}$$

where a is half the depth of the beam and r_0 is the radius of curvature of the neutral axis.

The numerical solutions are compared to the analytic solution in Fig. 5. Both of the finer meshes agree almost exactly with the analytic solution. Deformed configurations of the 20×2 mesh are shown in Fig. 6.

EXAMPLE 5.6. Mooney–Rivlin cylinder. A thick cylindrical cylinder as shown in Fig. 7 is subjected to internal pressure. Only one quarter of the whole structure is modelled by 10×1, 20×1, and 40×2 QBI elements. The analytic solution has been investigated by Rivlin [15]

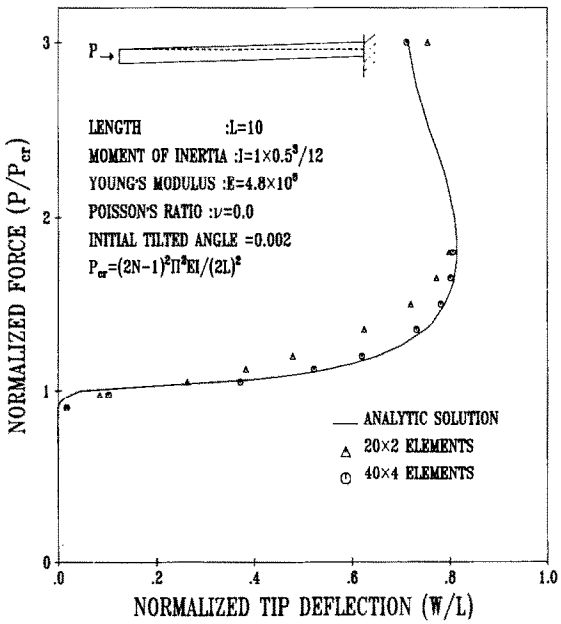

Fig. 4. Problem description and numerical results for Example 5.4: Post-buckling analysis of an imperfect column.

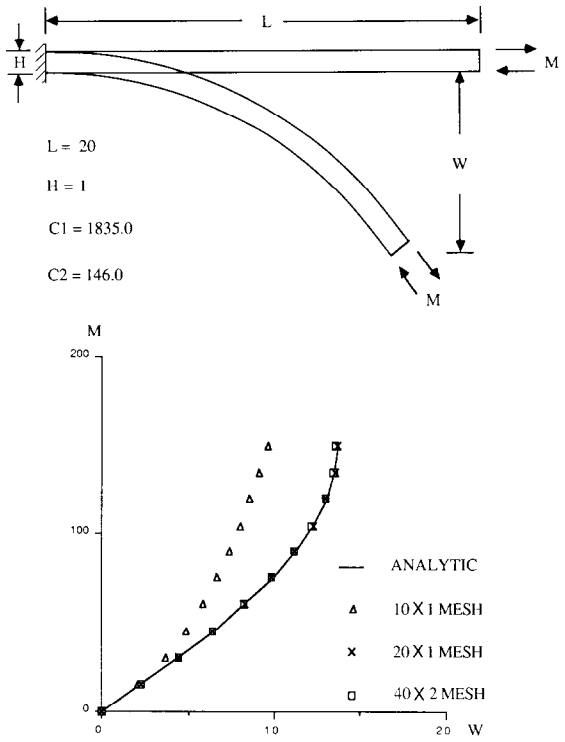

Fig. 5. Problem description and load-displacement curves of QBI element for Example 5.5: Mooney–Rivlin beam subjected to a tip moment.

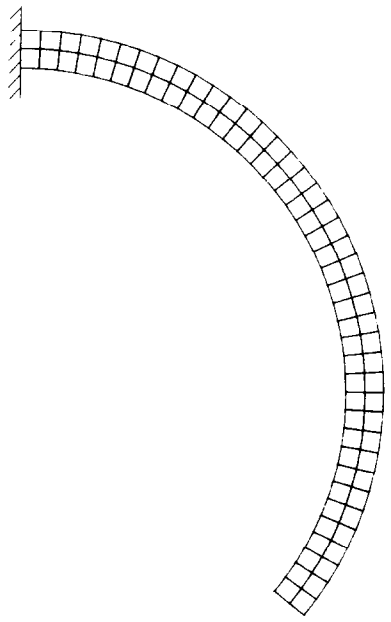

Fig. 6. The final deformed configuration for Example 5.5.

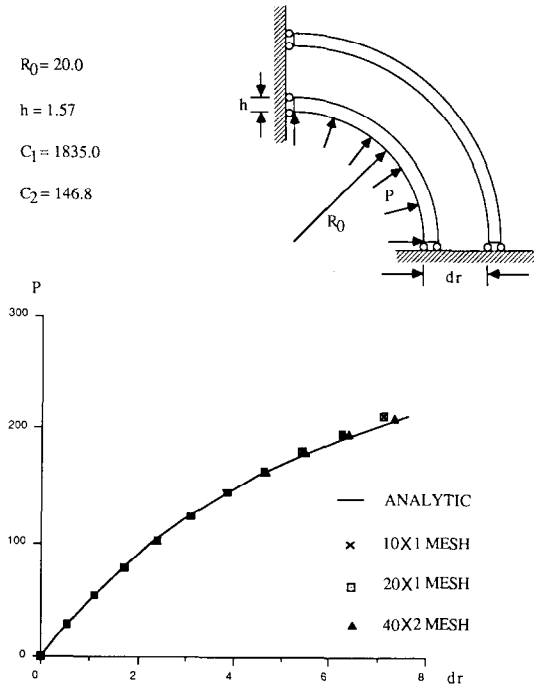

Fig. 7. Problem description and numerical results for Example 5.6: Mooney–Rivlin cylinder subjected to internal pressure.

where the internal pressure is given by

$$P(r_2) = (c_1 + c_2)\left[\frac{(r_2^2 - a_2^2)(a_1^2 - a_2^2)}{r_2^2(r_2^2 + a_1^2 - a_2^2)} + \ln\left(\frac{r_2^2}{r_2^2 + a_1^2 - a_2^2}\right) + \ln\frac{a_1^2}{a_2^2}\right], \tag{5.14}$$

in which a_1 and a_2 are the initial external and internal radii and r_2 is the internal radius after the cylinder is deformed.

The numerical solutions agree quite well with the analytic solution as shown in Fig. 7, even when a coarse mesh is used.

6. Conclusions

A formulation has been given for a flexurally superconvergent element which is applicable to problems involving geometrical and material nonlinearities. The linearized and the initial stress (geometric) stiffness matrices have been developed in a form consisting of the sum of a one-point quadrature and a stabilization matrix. The geometric stabilization matrix possesses the same structure as the linear matrix, consisting of terms of the form $\gamma\gamma^t$.

A study of the performance of this element in the nonlinear regime reveals that while it surpasses elements such as those based on selective reduced integration, the performance of the element does deteriorate somewhat in the nonlinear regime.

Appendix A

The coefficients which appeared in the expressions of $\boldsymbol{K}^D$ and $\bar{\boldsymbol{D}}$ are given by

$$c_1^D = \frac{H_{XX}H_{YY}}{\alpha^2}\left[\tilde{\alpha}_{XX}^D H_{XX}^2 H_{YY} + \bar{\nu}H_{XX}H_{XY}^2(\tilde{\alpha}_{XY}^D + \tilde{\alpha}_{YX}^D) + \bar{\nu}^2\tilde{\alpha}_{YY}^D H_{XX}H_{XY}^2\right], \tag{A.1}$$

$$c_2^D = \frac{H_{XX}H_{YY}}{\alpha^2}\left[H_{XX}H_{XY}H_{YY}(\tilde{\alpha}_{YX}^D + \bar{\nu}\tilde{\alpha}_{XX}^D + \bar{\nu}\tilde{\alpha}_{YY}^D) + \bar{\nu}^2\tilde{\alpha}_{XY}^D H_{XY}^3\right], \tag{A.2}$$

$$c_3^D = \frac{H_{XX}H_{YY}}{\alpha^2}\left[\tilde{\alpha}_{YY}^D H_{XX}H_{YY}^2 + \bar{\nu}H_{XY}^2 H_{YY}(\tilde{\alpha}_{XY}^D + \tilde{\alpha}_{YX}^D) + \bar{\nu}^2\tilde{\alpha}_{XX}^D H_{XY}^2 H_{YY}\right], \tag{A.3}$$

where

$$\alpha = H_{XX}H_{YY} - \bar{\nu}^2 H_{XY}^2, \tag{A.4}$$

$$\tilde{\alpha}_{XX}^D = \tilde{D}_{11} - \bar{\nu}(\tilde{D}_{12} + \tilde{D}_{21}) + \bar{\nu}^2\tilde{D}_{22}, \tag{A.5}$$

$$\tilde{\alpha}_{XY}^D = \tilde{D}_{12} - \bar{\nu}(\tilde{D}_{11} + \tilde{D}_{22}) + \bar{\nu}^2\tilde{D}_{21}, \tag{A.6}$$

$$\tilde{\alpha}_{YX}^D = \tilde{D}_{21} - \bar{\nu}(\tilde{D}_{11} + \tilde{D}_{22}) + \bar{\nu}^2\tilde{D}_{12}, \tag{A.7}$$

$$\tilde{\alpha}_{YY}^D = \tilde{D}_{22} - \bar{\nu}(\tilde{D}_{12} + \tilde{D}_{21}) + \bar{\nu}^2\tilde{D}_{11}. \tag{A.8}$$

The coefficients which appeared in the expressions of $\boldsymbol{K}^G$ and $\bar{\boldsymbol{T}}$ are similarly defined as above, with the superscript D replaced by G, and the $\tilde{D}_{\alpha\beta}$ components replaced by the $\tilde{T}_{\alpha\beta}$ components.

The c_4 and c_5 coefficients for the f_{stab} are

$$c_4 = \frac{H_{XX}}{\alpha}(H_{YY}q_5 + \bar{\nu}H_{XY}q_6), \tag{A.9}$$

$$c_5 = \frac{H_{YY}}{\alpha}(\bar{\nu}H_{XY}q_5 + H_{XX}q_6). \tag{A.10}$$

Acknowledgment

The support of the U.S. Army Research Office under Contract DAAG29-84-K-0057 and the support of the National Science Foundation for one of the authors (WKL) under Grant ECE-8420735 are gratefully acknowledged.

References

[1] E.L. Wilson, R.L. Taylor, W.P. Doherty and J. Ghaboussi, Incompatible displacement models, in: S.J. Fenves et al., eds., Numerical and Computer Methods in Structural Mechanics (Academic Press, New York, 1973) 43–58.

[2] R.L. Taylor, P.J. Beresford and E.L. Wilson, A non-conforming element for stress analysis, Internat. J. Numer. Meths. Engrg. 10 (1976) 1211–1219.
[3] M. Fröier, L. Nilsson and A. Samuelsson, The rectangular plane stress element by Turner, Pian and Wilson, Internat. J. Numer. Meths. Engrg. 8 (1974) 433–437.
[4] T. Belytschko and W.E. Bachrach, Efficient implementation of quadrilaterals with high coarse-mesh accuracy, Comput. Meths. Appl. Mech. Engrg. 54 (1986) 279–301.
[5] T. Belytschko, J.S.-J. Ong, W.K. Liu and J.M. Kennedy, Hourglass control in linear and nonlinear problems, Comput. Meths. Appl. Mech. Engrg. 43 (1984) 251–276.
[6] K. Washizu, Variational Methods in Elasticity and Plasticity (Pergamon Press, Oxford, 1968).
[7] S. Nemat-Nasser, On variational methods in finite and incremental elastic deformation problems with discontinuous fields, Quart. Appl. Math. 30 (1972) 143–156.
[8] W.K. Liu, J.S.-J. Ong and R.A. Uras, Finite element stabilization matrices – a unification approach, Comput. Meths. Appl. Mech. Engrg. 53 (1985) 13–46.
[9] W.K. Liu, T. Belytschko, J.S.-J. Ong and S.E. Law, Use of stabilization matrices in non-linear analysis, Engrg. Computat. 2 (1985) 47–55.
[10] S.P. Timoshenko and J.M. Gere, Mechanics of Materials (Van Nostrand Reinhold, New York, 1972) 208–211.
[11] T. Belytschko and L.W. Glaum, Applications of higher order corotational stretch theories to nonlinear finite element analysis, Comput. & Structures 10 (1979) 175–182.
[12] H.L. Schreyer and E.F. Masur, Buckling of shallow arches, ASCE J. Engrg. Mech. Div. EM4 (1966) 1–19.
[13] S.P. Timoshenko and J.M. Gere, Theory of Elastic Stability (McGraw-Hill, New York, 2nd ed., 1961) 76–82.
[14] R.S. Rivlin, Large elastic deformations of isotropic materials. Part V, the problem of flexure, Proc. Roy. Soc. London, A195 (1949) 463–473.
[15] R.S. Rivlin, Large elastic deformations of isotropic materials. Part VI, further results in the theory of torsion, shear and flexure, Philos. Trans. Roy. Soc. London A242 (1949) 173–195.